Direct observation of resonance scattering patterns in single silicon nanoparticles

Vytautas Valuckas, Ramón Paniagua-Domínguez, Yuan Hsing Fu, Boris Luk'yanchuk, and Arseniy I. Kuznetsov[a)]
*Data Storage Institute, A*STAR (Agency for Science, Technology and Research), 2 Fusionopolis Way, #08-01, Innovis, Singapore 138634*

(Received 14 November 2016; accepted 15 February 2017; published online 1 March 2017)

We present the first direct observation of the scattering patterns of electric and magnetic dipole resonances excited in a single silicon nanosphere. Almost perfectly spherical silicon nanoparticles were fabricated and deposited on a 30 nm-thick silicon nitride membrane in an attempt to minimize particle—substrate interaction. Measurements were carried out at visible wavelengths by means of the Fourier microscopy in a dark-field illumination setup. The obtained back-focal plane images clearly reveal the characteristic scattering patterns associated with each resonance and are found to be in a good agreement with the simulated results. *Published by AIP Publishing.*
[http://dx.doi.org/10.1063/1.4977570]

Light scattering by small particles is an important physical process playing a central role in a wide variety of applications such as surface enhanced spectroscopies and sensing,[1] photovoltaics[2] or optical communications[3] to name a few. Two of those gathering increasing attention are metasurfaces[4] and nanoantennas for quantum emitters (efficient near-to-far field transducers modifying their radiative characteristics and radiation patterns[5,6]). While traditionally designed using plasmonic materials, nanoantennas and metasurfaces are now showing a trend of shifting towards dielectric materials due to their lower dissipative losses in the visible spectral range and CMOS compatibility, which is beneficial for many applications.[7–23] Additionally, nanoantennas made of high refractive index dielectrics, unlike plasmonic ones, may support magnetic resonances even when shaped in the simple form of spheres. For example, it follows from the Mie theory[24,25] and has been experimentally demonstrated[26–28] that silicon (Si) spheres of 100–200 nm in diameter have clearly separated dipole resonances in the visible. For these systems, the first and second lowest-energy resonances correspond to the magnetic dipole (MD) and electric dipole (ED), respectively. The interference of the new family of magnetic modes with the usual electric ones bring interesting associated effects such as the backscattering suppression (so called first Kerker condition).[24,29–35]

In describing dielectric resonators as nanoantennas, both the directivity (radiation pattern) and gain (total efficiency) are important parameters. The former, however, has been the subject of much less experimental study, with only a few exceptions.[32,36] For this purpose, the Fourier microscopy has proved to be a powerful technique allowing precise measurements of the emission[37–42] or scattering[43–45] directivity in the far field. This paper reports the first direct experimental imaging of the scattering patterns associated with the ED and MD resonances excited in single dielectric nanospheres. Almost perfectly spherical nanoparticles (NP) of different diameters were fabricated by laser ablation and deposited on top of a 30 nm thick silicon nitride (SiN) membrane. In these conditions, the impact of the environment is minimized and nanospheres scatter light almost accordingly to the free-standing case. The experimental data were obtained using a dark field microscope capturing images in the Fourier plane and compared to the numerical simulations, showing a very good agreement.

The spherical Si NP were deposited on the SiN membrane using the laser-induced transfer (LIT) method.[33,46] For that, 1 kHz femtosecond laser system (Tsunami + Spitfire, Spectra Physics) delivering 1 mJ, 100 fs laser pulses at central wavelength of 800 nm was used. The laser beam was focused using a 100× long working distance objective lens (Mitutoyo M Plan Apo NIR 100×, NA 0.5) onto a crystalline Si substrate through a quartz slide. The laser beam power was attenuated by a filter, a polarizer and a halfwave plate to achieve a final fluence of about 0.6 J/cm^2 at the Si surface. The wafer was ablated, and Si NP of various sizes were deposited on the quartz slide. Si NP were subsequently transferred further from the quartz slide to a 30 nm-thick SiN membrane using a similar technique. The laser beam was shaped into a square-shaped flat-top profile with the size of $15 \times 15\ \mu m^2$ using an image transfer of $300 \times 300\ \mu m^2$ pinhole with a tube lens and a 20× long working distance objective lens (Olympus S Plan NIC 20×, NA 0.4).[47] The laser beam was attenuated to deliver about 0.2 J/cm^2 at the sample surface. We scanned the laser beam through the quartz slide with the Si particles on its bottom surface and the SiN membrane under it to detach the particles from the quartz and drop them onto the membrane.

Particles were imaged using SEM (SU8220, Hitachi) and characterized by measuring their forward scattering spectra (Fig. 1(a)). For that purpose, an optical dark-field microscope (Nikon, Ti-U) equipped with a high-sensitivity spectrometer (Andor SR-303i) and a 400×1600 pixel EMCCD (Andor Newton) was used. A dark field condenser was applied to illuminate the particles through the membrane, and their forward scattered light was collected with 100× dark field microscope objective (Nikon LU Plan 100×, NA 0.8).[26]

[a)]Electronic mail: arseniy_k@dsi.a-star.edu.sg

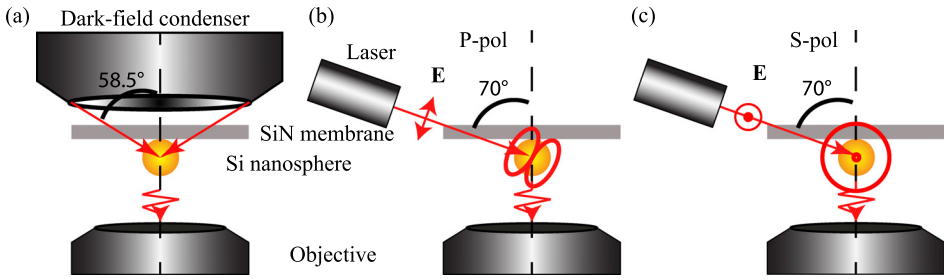

FIG. 1. Experimental setup for forward scattering spectra measurements (a) and scattering directivity measurements (b), (c).

For the experiment, we selected two particles, one with diameter D around 180 nm (Fig. 2(a), top-right panel) and having clearly separated ED and MD resonances in the visible spectral range (Fig. 2(a), top-left panel) and the other with D around 105 nm (Fig. 2(b), top-right panel) and only MD in the visible range (Fig. 2(b), top-left panel). Numerical simulations were performed following the experimental configuration, i.e., 58.5° oblique incidence illumination from the SiN membrane side and spectrum collection in transmission only (NA = 0.8). Unpolarized light is obtained averaging over *p*- and *s*-polarizations. A detailed description of the numerical simulation can be found in the supplementary materials. The best correspondence with the experiment is found for particle sizes of 178 nm and 105 nm, as shown in the bottom-left panels in Figs. 2(a) and 2(b), respectively.

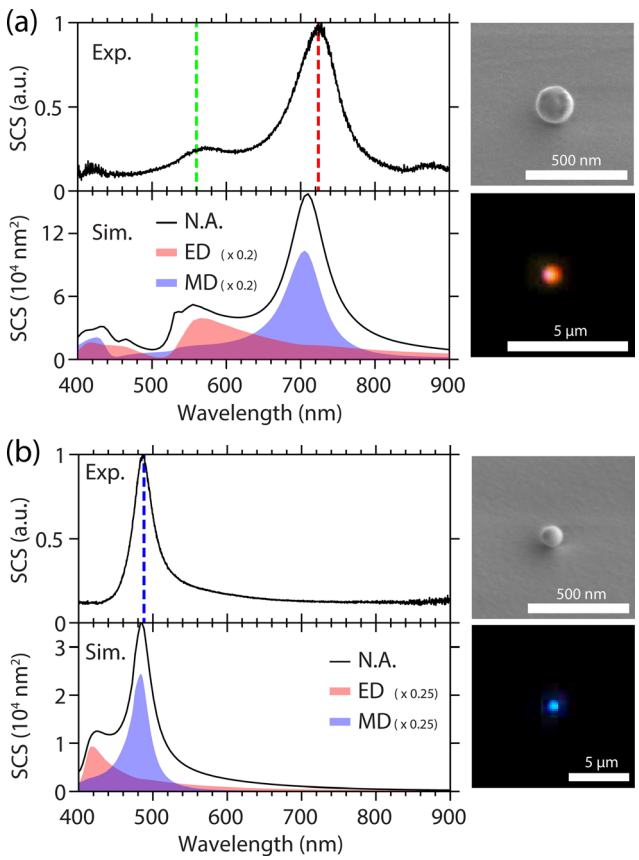

FIG. 2. Experimental forward scattering spectra (top) and simulated forward scattering cross sections collected with a numerical aperture of 0.8 (N.A.) (bottom) of a Si nanosphere with (a) D = 180 nm (178 nm in simulation) and (b) D = 105 nm on a SiN membrane (30 nm thickness). Blue and red shaded areas in the simulations show, respectively, the contributions of magnetic and electric dipoles to the total SCS. Top- and bottom-right panels in (a) and (b) show, respectively, the SEM and dark-field microscope images of the measured particles.

The ED and MD character of the resonances observed is corroborated performing a multipolar decomposition of the polarization currents inside the particles.[15,23] While the scattering cross section (SCS) of the particle was calculated integrating the Poynting's vector on the solid angle corresponding to the numerical aperture of the objective used in the experiment, multipolar contributions correspond to the total emitted power and are, therefore, scaled by the indicated factors to allow a simple comparison of the resonance peak positions. The results are shown as shaded, colored areas, from which the character of the different resonances can be clearly identified. While, according to the simulations, the smaller sphere should also show a peak for the electric dipole mode, it is not seen in the measured spectra due to the limited range of the detector used.

To observe the radiation patterns associated with the induced dipoles in the nanospheres, we placed a CCD camera in the back focal plane of the collection objective. A supercontinuum laser (SuperK Power, NKT Photonics) and a continuous wave (CW) diode laser with a wavelength of 488 nm (PhoxX, Omicron-Laserage) were used to illuminate the particles through the membrane (Figs. 1(b) and 1(c)) at an angle (70°) at wavelengths coinciding with the resonance peaks. Both *p*- and *s*-polarizations were used to image the dipole emission with different dipole moment orientations. Intensity maps are extracted by converting the red-green-blue (RGB) images into grayscale according to the Bayer filter transmission spectral profiles at the corresponding wavelengths. These Fourier space images represent the angular intensity distributions of emission towards the objective. In this configuration, it is possible to distinguish the ED and MD orientation by imaging the radiation patterns obtained with the *p*- and *s*-polarizations. Note that for a dipole radiating in a homogeneous medium, its radiation pattern corresponds to a torus with its axis aligned with the dipole moment axis. Also note that different polarizations induce different dipole moment orientations, as illustrated with the ED case in Figures 1(b) and 1(c). Numerical simulations were carried out to check the validity of the measured radiation patterns. For that, we separately simulated the *p*- and *s*-polarized oblique plane wave excitation (70° from the membrane side) and recorded the scattering far-field in the forward direction with the same NA restriction (0.8). The simulations of free-standing spheres were also carried out for comparison. The results are presented in the supplementary material, Figure S1.

Let us start analyzing the scattering directivity results for the particle with D = 180 nm. As shown in Figure 3, the patterns show a clear distinction between *p*-and *s*-polarizations, corresponding to dipoles in orthogonal orientations. We first focus on the ED resonance case (Figs. 3(a)–3(d)), for which

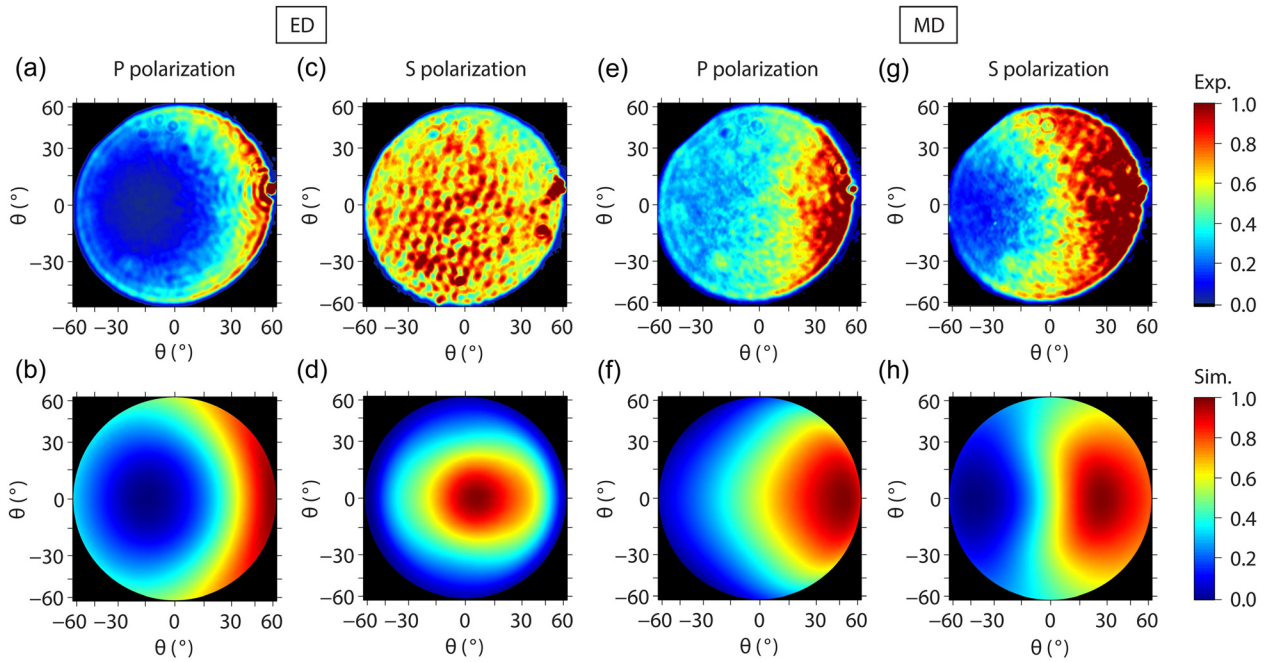

FIG. 3. Experimental and simulated back focal plane images representing the scattering diagrams of the Si particle (D = 180 nm) at 590 nm (a)–(d) and 710 nm (e)–(h) wavelengths for *p*- ((a), (b) and (e), (f)) and *s*-polarizations ((c), (d) and (g), (h)).

the MD contribution is weak. In the case of *p*-polarization, the ED is contained in the plane of incidence. Note that in the case of a homogeneous environment (see supplementary material, Fig. S1), the ED is tilted from the optical axis of the objective by 20°. In the case of a single dipole, it would be exactly 20; thus, the impact of the MD is low. This tilting is clearly observed as a minimum towards the objective in the scattering pattern in our experimental configuration (Fig. 3(a)). The small deviation in the position of the minimum from 20° evidences the small influence of the 30 nm-thick SiN membrane in this case. Simultaneously, maximum scattering is observed at the edges, as expected from theory and simulations (Fig. 3(b)). For *s*-polarization (Figs. 3(c) and 3(d)), the ED is perpendicular to the incidence plane (parallel to the substrate) and no obvious minimum in scattering pattern is observed, as expected (for a homogeneous environment, the pattern would correspond to a side view of the radiation torus). Note, however, that simulations predict a larger influence of the membrane for this dipole orientation, evidenced as a decrease of the intensity towards the edge of the image. In the MD resonance case (Figs. 3(e)–3(h)), the situation is the opposite with the MD being orthogonal (parallel) to the incidence plane for *p*-polarized (*s*-polarized) excitation. Again, in a homogeneous environment, the dipole would be tilted by 20° with respect to the optical axis for *s*-polarized excitation, causing a minimum in the radiation pattern at approximately this angle (the slight deviation being caused by the ED contribution). While there is, still, an obvious difference in the scattering pattern between the *s*- and *p*-polarized excitations, the SiN membrane has a more pronounced influence in these results, as predicted by simulations. This is a consequence of the different reflectivity for the *s*- and *p*-polarized light components from the membrane which, in turn, translates in a different impact on the radiation pattern of the different dipoles involved (ED or MD and parallel or perpendicular to the incidence plane). As a consequence, at 710 nm, the minimum towards the objective is not that obvious for *s*-polarization (Figs. 3(g) and 3(h)), as it was for the p-polarized case at 590 nm. For *p*-polarization, the deformation of the torus is more pronounced at 710 nm than it is at 590 nm, with an evident maximum on the side (Figs. 3(e) and 3(f)). This effect, which is also evident in the free-standing case, follows from the different relative contributions of ED and MD at different wavelengths.

We note a systematic broadening of the patterns in the experiment, as compared with the simulations. This may be attributed to the deviations in the particle shape from a perfect sphere (as may be observed in the corresponding SEM) as well as in its material composition (the real sample being poly-crystalline but modelled as pure c-Si). This broadening does not have a very strong impact for those patterns having a minimum around the central region of the image (Figs. 3(a) and 3(b) and 3(g) and 3(h)) because all important features observed in simulations are reproduced in the experiment (in particular, the minima, which define their overall shape, can be clearly seen), but it has a stronger influence in those patterns in which the minima happen near the edges of the image (Figs. 3(c) and 3(d) and 3(e) and 3(f)).

In the case of the smaller particle (D = 105 nm), having only MD resonance in visible (Figure 4), similar results to those of the larger particle at MD resonance are expected. It is indeed the case, as evidenced comparing Figs. 4(a) and 4(b) and 3(e) and 3(g). The influence of the ED contribution (significant even in the free standing case) together with that of the SiN membrane makes the scattering pattern significantly depart from that of a single radiating dipole in a homogeneous environment. These experimental results, which are similar to those obtained for the larger particle, are in close agreement with the simulated ones (Figs. 4(c) and 4(d)).

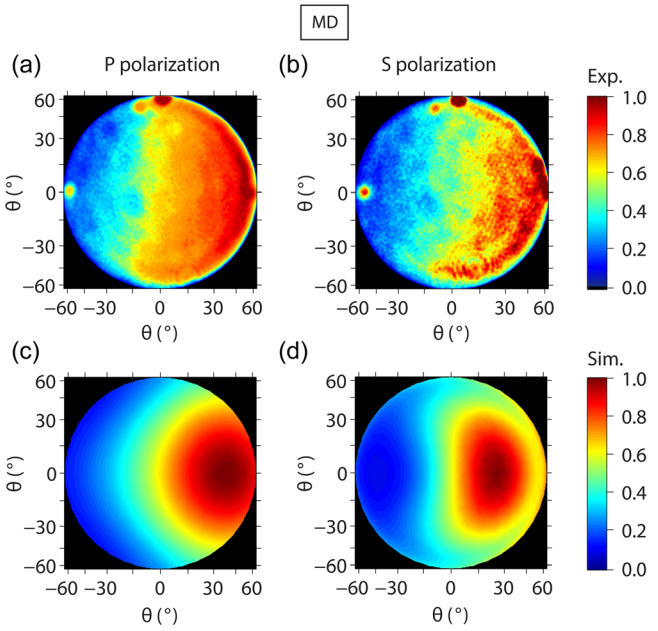

FIG. 4. Back focal plane images representing the scattering diagrams of the smaller Si particle (D = 105 nm) at 488 nm for (a) *p*- and (b) *s*-polarizations. (c), (d) Corresponding simulated results.

Note that in Figs. 3 and 4, all intensities are self-normalized for P and S polarizations. The reason for doing so, instead of using the same scale, is that the signal is much lower for the S polarized case. The reason behind this difference in intensities is the higher reflectivity of the membrane for S polarized light. As a consequence of this higher reflectivity, the light intensity actually reaching the particle is much lower in the S polarized case, and so it is the signal in the back focal plane for this polarization. The difference in the speckle intensity observed between the images of Figs. 3 and 4 is due to the different light sources and different cameras used for the measurements.

In conclusion, we present the first direct experimental observation of the radiation patterns of electric and magnetic dipole resonances in silicon nanospheres. These were fabricated by laser ablation and deposited on a 30 nm-thick SiN membrane to minimize the impact of the substrate on their optical properties. The SEM images of the particles were correlated with their individual (forward) scattering spectra in a dark field configuration. The scattering patterns were measured using the Fourier microscopy, and the induced dipole orientation identified rotating the polarization of the exciting laser. While purely dipolar patterns were observed at the electric dipole resonance position, corroborating the negligible impact of the SiN membrane and the magnetic (and higher order) contributions, scattering patterns of the magnetic dipole resonance are more affected by both the membrane and the electric dipole contribution, as expected. This study provides an experimental observation of the radiation characteristics of silicon particles in the visible and corroborates the power of Fourier microscopy for nanoantenna characterization.

See supplementary material for a comparison of the presented results with the free standing particle case and further details about the numerical simulations.

The authors were supported by the DSI core funds and the A*STAR SERC Pharos program, Grant No. 152 73 00025 (Singapore).

[1]A. J. Haes, C. L. Haynes, A. D. McFarland, G. C. Schatz, R. P. Van Duyne, and S. Zou, MRS Bull. **30**, 368 (2005).
[2]H. A. Atwater and A. Polman, Nat. Mater. **9**, 205 (2010).
[3]E. Ozbay, Science **311**, 189 (2006).
[4]N. Yu and F. Capasso, Nat. Mater. **13**, 139 (2014).
[5]L. Novotny and N. Van Hulst, Nat. Photonics **5**, 83 (2011).
[6]V. Giannini, A. I. Fernandez-Domínguez, S. C. Heck, and S. A. Maier, Chem. Rev. **111**, 3888 (2011).
[7]A. I. Kuznetsov, A. E. Miroschnichenko, M. L. Brongersma, Y. S. Kivshar, and B. Luk'yanchuk, Science **354**, aag2472 (2016).
[8]J. A. Schuller and M. L. Brongersma, Opt. Express **17**, 24084 (2009).
[9]B. Rolly, B. Stout, and N. Bonod, Opt. Express **20**, 20376 (2012).
[10]M. K. Schmidt, R. Esteban, J. Sáenz, I. Suárez-Lacalle, S. Mackowski, and J. Aizpurua, Opt. Express **20**, 13636 (2012).
[11]P. Albella, M. A. Poyli, M. K. Schmidt, S. A. Maier, F. Moreno, J. J. Sáenz, and J. Aizpurua, J. Phys. Chem. C **117**, 13573 (2013).
[12]D. Lin, P. Fan, E. Hasman, and M. L. Brongersma, Science **345**, 298 (2014).
[13]P. Albella, R. Alcaraz de la Osa, F. Moreno, and S. A. Maier, ACS Photonics **1**, 524 (2014).
[14]M. Decker, I. Staude, M. Falkner, J. Dominguez, D. N. Neshev, I. Brener, T. Pertsch, and Y. S. Kivshar, Adv. Opt. Mater. **3**, 813 (2015).
[15]Y. F. Yu, A. Y. Zhu, R. Paniagua-Domínguez, Y. H. Fu, B. Luk'yanchuk, and A. I. Kuznetsov, Laser Photonics Rev. **9**, 412 (2015).
[16]M. I. Shalaev, J. Sun, A. Tsukernik, A. Pandey, K. Nikolskiy, and N. M. Litchinitser, Nano Lett. **15**, 6261 (2015).
[17]K. E. Chong, I. Staude, A. James, J. Dominguez, S. Liu, S. Campione, G. S. Subramania, T. S. Luk, M. Decker, D. N. Neshev, I. Brener, and Y. S. Kivshar, Nano Lett. **15**, 5369 (2015).
[18]A. Arbabi, Y. Horie, M. Bagheri, and A. Faraon, Nat. Nanotechnol. **10**, 937 (2015).
[19]R. M. Bakker, D. Permyakov, Y. F. Yu, D. Markovich, R. Paniagua-Domínguez, L. Gonzaga, A. Samusev, Y. Kivshar, B. Luk'yanchuk, and A. I. Kuznetsov, Nano Lett. **15**, 2137 (2015).
[20]U. Zywietz, M. K. Schmidt, A. B. Evlyukhin, C. Reinhardt, J. Aizpurua, and B. N. Chichkov, ACS Photonics **2**, 913 (2015).
[21]P. Moitra, B. A. Slovick, W. Li, I. I. Kravchencko, D. P. Briggs, S. Krishnamurthy, and J. Valentine, ACS Photonics **2**, 692 (2015).
[22]M. Caldarola, P. Albella, E. Cortés, M. Rahmani, T. Roschuk, G. Grinblat, R. F. Oulton, A. V. Bragas, and S. A. Maier, Nat. Commun. **6**, 7915 (2015).
[23]R. Paniagua-Domínguez, Y. F. Yu, A. E. Miroshnichenko, L. A. Krivitsky, Y. H. Fu, V. Valuckas, L. Gonzaga, Y. T. Toh, A. Y. S. Kay, B. Luk'yanchuk, and A. I. Kuznetsov, Nat. Commun. **7**, 10362 (2016).
[24]A. B. Evlyukhin, C. Reinhardt, A. Seidel, B. S. Luk'yanchuk, and B. N. Chichkov, Phys. Rev. B **82**, 045404 (2010).
[25]A. García-Etxarri, R. Gómez-Medina, L. S. Froufe-Pérez, C. López, L. Chantada, F. Scheffold, J. Aizpurua, M. Nieto-Vesperinas, and J. J. Sáenz, Opt. Express **19**, 4815 (2011).
[26]A. I. Kuznetsov, A. E. Miroshnichenko, Y. H. Fu, J. Zhang, and B. Luk'yanchuk, Sci. Rep. **2**, 492 (2012).
[27]A. B. Evlyukhin, S. M. Novikov, U. Zywietz, R. L. Eriksen, C. Reinhardt, S. I. Bozhevolnyi, and B. N. Chichkov, Nano Lett. **12**, 3749 (2012).
[28]L. Shi, T. U. Tuzer, R. Fenollosa, and F. Meseguer, Adv. Mater. **24**, 5934 (2012).
[29]M. Kerker, D.-S. Wang, and C. Giles, J. Opt. Soc. Am. **73**, 765 (1983).
[30]M. Nieto-Vesperinas, R. Gómez-Medina, and J. Sáenz, J. Opt. Soc. Am. A **28**, 54 (2011).
[31]R. Gómez-Medina, B. García-Cámara, I. Suárez-Lacalle, F. González, F. Moreno, M. Nieto-Vesperinas, and J. J. Sáenz, J. Nanophotonics **5**, 053512 (2011).
[32]J.-M. Geffrin, B. García-Cámara, R. Gómez-Medina, P. Albella, L. S. Froufe-Pérez, C. Eyraud, A. Litman, R. Vaillon, F. González, M. Nieto-Vesperinas, J. J. Sáenz, and F. Moreno, Nat. Commun. **3**, 1171 (2012).
[33]Y. H. Fu, A. I. Kuznetsov, A. E. Miroshnichenko, Y. F. Yu, and B. Luk'yanchuk, Nat. Commun. **4**, 1527 (2013).
[34]S. Person, M. Jain, Z. Lapin, J. J. Sáenz, G. Wicks, and L. Novotny, Nano Lett. **13**, 1806 (2013).
[35]B. S. Luk'yanchuk, N. V. Voshchinnikov, R. Paniagua-Domínguez, and A. I. Kuznetsov, ACS Photonics **2**, 993 (2015).

[36]T. Coenen, J. van de Groep, and A. Polman, ACS Nano **7**, 1689 (2013).
[37]A. G. Curto, G. Volpe, T. H. Taminiau, M. P. Kreuzer, R. Quidant, and N. F. van Hulst, Science **329**, 930 (2010).
[38]G. Grzela, R. Paniagua-Domínguez, T. Barten, Y. Fontana, J. A. Sánchez-Gil, and J. G. Rivas, Nano Lett. **12**, 5481 (2012).
[39]T. H. Taminiau, S. Karaveli, N. F. van Hulst, and R. Zia, Nat. Commun. **3**, 979 (2012).
[40]A. G. Curto, T. H. Taminiau, G. Volpe, M. P. Kreuzer, R. Quidant, and N. F. van Hulst, Nat. Commun. **4**, 1750 (2013).
[41]T. Coenen, F. B. Arango, A. F. Koenderink, and A. Polman, Nat. Commun. **5**, 3250 (2014).
[42]D. van Dam, D. R. Abujetas, R. Paniagua-Domínguez, J. A. Sánchez-Gil, E. P. Bakkers, J. E. Haverkort, and J. Gómez Rivas, Nano Lett. **15**, 4557 (2015).
[43]T. Shegai, S. Chen, V. D. Miljković, G. Zengin, P. Johansson, and M. Käll, Nat. Commun. **2**, 481 (2011).
[44]I. Sersic, C. Tuambilangana, and A. F. Koenderink, New J. Phys. **13**, 083019 (2011).
[45]T. Shegai, V. D. Miljković, K. Bao, H. Xu, P. Nordlander, P. Johansson, and M. Käll, Nano Lett. **11**, 706–711 (2011).
[46]A. Kuznetsov, J. Koch, and B. Chichkov, Opt. Express **17**, 18820 (2009).
[47]A. Kuznetsov, J. Koch, and B. Chichkov, Appl. Phys. A **94**, 221 (2009).